https://doi.org/10.3311/PPch.39479
Creative Commons Attribution

Periodica Polytechnica Chemical Engineering, 69(2), pp. 191–203, 2025

Synthesis and Characterization of SnO_2/S,N-Carbon Quantum Dots as Photoelectrochemical Water Splitting Material

Nanda Destiyana[1], Liszulfah Roza[2], Nonni Soraya Sambudi[1*], Vivi Fauzia[3], Suriati Sufian[4], Sylvia Ayu Pradanawati[5], Resista Vikalina[6], Yose Fachmi Buys[5]

[1] Department of Chemical Engineering, Faculty of Industrial Technology, Universitas Pertamina, Jl. Teuku Nyak Arief, 12220 Jakarta, Indonesia
[2] Research Center for Nanotechnology System (PRSN), Research Organization of Nanotechnology and Material (ORNM), National Research and Innovation Agency (BRIN), Gedung B.J. Habibie, Jl. M.H. Thamrin No. 8, 10340 Jakarta Pusat, Indonesia
[3] Department of Physics, Faculty of Mathematics and Natural Sciences, Universitas Indonesia, 16424 Depok, Indonesia
[4] Chemical Engineering Department, Faculty of Engineering, Universiti Teknologi PETRONAS, 32610 Seri Iskandar, Perak, Malaysia
[5] Department of Mechanical Engineering, Faculty of Industrial Technology, Universitas Pertamina, Jl. Teuku Nyak Arief, 12220 Jakarta, Indonesia
[6] Department of Logistics Engineering, Faculty of Industrial Technology, Universitas Pertamina, Jl. Teuku Nyak Arief, 12220 Jakarta, Indonesia
* Corresponding author, e-mail: nonni.ss@universitaspertamina.ac.id

Received: 03 December 2024, Accepted: 16 May 2025, Published online: 05 June 2025

Abstract

Given the growing global demand for renewable energy and the need for sustainable hydrogen production, the development of efficient photoelectrochemical systems for water splitting has become a critical area of research in addressing the energy crisis and reducing greenhouse gas emissions. This study investigates the synthesis of SnO_2 thin film photoanodes using ultrasonic spray pyrolysis (USP) and hydrothermal methods, with the aim of evaluating the effects of S,N-carbon quantum dot (CQD) modification on photoelectrochemical performance. The S,N-CQDs solution was varied in volume (2.5, 5, 7.5, and 10 mL) and applied to the SnO_2 thin films. The resulting SnO_2 microstructure exhibited a spherical morphology with distinct atomic concentrations of Sn and O. Photoelectrochemical characterization, performed via linear sweep voltammetry (LSV) and cyclic voltammetry (CV), demonstrated that the SnO_2 thin film modified with 7.5 mL of S,N-CQDs solution produced the highest photocurrent density of 0.0356 mA/cm^2, along with an optimal photoconversion efficiency (PCE) of 0.0084%. Furthermore, the SnO_2/S,N-CQDs photoanode with 7.5 mL of S,N-CQDs exhibited a double-layer capacitance (C_{dl}) of 0.1175 mF/cm^2, indicating enhanced electrochemical active sites. These findings suggest that the incorporation of S,N-CQDs into SnO_2 thin films effectively increases the active surface area, thereby improving the efficiency of the photoelectrochemical water splitting process.

Keywords

SnO_2, carbon quantum dots, thin film, photoelectrochemical water splitting

1 Introduction

The energy crisis and climate change are pressing global issues, with rising greenhouse gas emissions severely impacting both human life and the environment. To address these challenges, prioritizing energy efficiency, transitioning to more sustainable resources, and reducing pollution are essential for energy conservation. Hydrogen presents a promising solution to lower greenhouse gas emissions and support global environmental management. As an efficient and abundant alternative energy source, hydrogen can play a key role in reducing emissions and fostering a sustainable future [1, 2]. Currently, hydrogen is primarily produced through industrial processes like coal gasification, which relies on fossil fuels such as natural gas and coal. This method is favored due to its higher energy yields and lower production costs [3]. However, fossil fuel-based production releases harmful greenhouse gases, such as carbon dioxide and methane, which pose significant threats to the environment [4–6]. Photoelectrochemical water splitting (PEC-WS), which harnesses the unlimited energy of sunlight, has emerged

Cite this article as: Destiyana, D., Roza, L., Sambudi, N. S., Fauzia, V., Sufian, S., Pradanawati, S. A., Vikalina, R., Buys, Y. F. "Synthesis and Characterization of SnO_2/S,N-Carbon Quantum Dots as Photoelectrochemical Water Splitting Material", Periodica Polytechnica Chemical Engineering, 69(2), pp. 191–203, 2025. https://doi.org/10.3311/PPch.39479

as a promising method for hydrogen production. PEC-WS is an environmentally friendly and sustainable process that converts solar energy into chemical energy, such as hydrogen, by using semiconductor materials. This process involves two key reactions: the hydrogen evolution reaction (HER) for water reduction and the oxygen evolution reaction (OER) for water oxidation [7, 8]. Carbon quantum dots (CQDs) are a promising approach to enhance the efficiency of PEC-WS and address its challenges. They help improve the spectral emission of samples with wide band gaps, thereby boosting performance [9]. CQDs offer several advantages, including high fluorescence intensity, excellent optical properties, good biocompatibility, stable chemical behavior, and environmental harmlessness. They are also cost-effective, water-soluble, inert, low in toxicity, easy to synthesize, and straightforward to apply [10–12]. From a physics standpoint, the electronic energy spectrum of CQDs resembles that of a direct bandgap semiconductor. Consequently, CQDs have been proposed as fluorescent materials for use in advanced optical and optoelectronic devices [3, 13]. With active surface groups such as –OH and $–CO_2H$, CQDs can be functionalized and combined with other organic or inorganic materials, enabling a wide range of innovative applications [14]. N-doped CQDs and nitrogen/sulfur co-doped CQDs (N,S-CQDs) exhibit significantly higher fluorescence quantum efficiency and photocatalytic activity compared to pure CQDs [15, 16]. Additionally, the improved performance of N-doped CQDs has been positively correlated with the extent of nitrogen doping [17, 18]. Previous study on SnO_2 with carbon doping exhibited high yield of hydrogen evolution at around 38.4 μmol/g h from water splitting process [19]. While the embedment of CQDs in SnO_2 has shown improvement in light absorption which increases the photocatalytic activity [20].

In this study, a new, efficient, and stable visible light-driven photocatalyst (CQD-surface modified SnO_2 nanoparticles) is prepared using ultrasonic spray pyrolysis (USP) to deposit CQDs onto the surface of SnO_2 nanoparticles, which are then used for PEC-WS. The CQDs are derived from organic materials, such as sucrose, fruit juices, peels, grasses, and plant leaves [21]. *Egeria densa* is an example of an organic material that can be used to produce CQDs, as it is a non-food resource and an invasive species [22].

2 Experimental

2.1 Materials

$SnCl_2{\cdot}2H_2O$ on fluorine-doped tin oxide (FTO) substrates (Merck, USA), HCl (Merck, USA) and NaOH (Merck, USA) was used as stabilizer. Synthesis of S,N-CQDs from *Egeria densa* algae, with the sulfur and nitrogen components derived from Na_2SO_4 (Merck, USA) and NH_4OH (Merck, USA).

2.2 Synthesis of tin oxide

The synthesis of SnO_2 on FTO substrates involves two stages: seeding and growth. In this study, the seeding process was performed using the USP method. The precursor solution was prepared by dissolving 0.2 M $SnCl_2{\cdot}2H_2O$ in a mixture of deionized (DI) water and HCl. HCl was added drop by drop to the $SnCl_2$ solution until the pH reached 1, followed by stirring for 30 min using a magnetic stirrer. The precursor solution was then sprayed onto the FTO substrate using a nebulizer at a substrate temperature of 450 °C. The substrate was first cleaned and sterilized sequentially with acetone, isopropanol, and DI water. During the spraying process, the substrate temperature was maintained using a hotplate, and spraying continued for 15 min. After spraying, the film was placed on a Petri dish and allowed to cool gradually to room temperature.

After seeding the FTO substrate, the sample was grown using the hydrothermal method. A total of 0.3966 g of $SnCl_2{\cdot}2H_2O$ (99%) and 0.5686 g of NaOH (99%) as precursors were dissolved separately in 28 mL DI water. The NaOH solution was added drop by drop to the $SnCl_2$ solution until the pH reached 13. The combined precursor solution was then transferred into a stainless-steel, teflon-lined autoclave, with the seeded FTO substrate placed in the solution, conductive surface facing upward. The autoclave was placed in an oven at 210 °C for 24 h. Afterward, the SnO_2 thin film was cleaned multiple times with DI water and annealed at 450 °C in a furnace under atmospheric conditions for 2 h [16].

2.3 Synthesis of S,N-CQDs

Before synthesizing CQDs from algae, a pre-treatment step is necessary to remove soil because soil is a habitation for algae evolution [23]. First, the algae were thoroughly cleaned, washed with water, and then dried. A sample of 3 g of algae was mixed with 100 mL of a 0.1 M sodium sulfate and 0.1 M ammonium hydroxide solution. The algae were then placed in a mortar and crushed. The refined algae, now dissolved in the sodium sulfate-ammonium hydroxide solution, were transferred to a beaker or Erlenmeyer flask and placed into a stainless-steel, teflon-lined autoclave. The autoclave is then heated in an oven at 250 °C for 3 h. During this time, the algae solution underwent a color change to brown.

The mixture is filtered using filter paper and centrifuged to separate the solution. The resulting solution is then prepared for coating onto the SnO_2 thin film.

2.4 Synthesis of SnO_2/S,N-CQDs

The SnO_2 thin film samples were annealed and then coated with S,N-CQDs derived from algae. The S,N-CQDs solution was applied to the SnO_2 surface using the spray pyrolysis method. In this process, the solution was sprayed onto the sample with varying volumes of 2.5 mL, 5 mL, 7.5 mL, and 10 mL. The spray tool was positioned above the sample, with a nozzle-to-sample distance of approximately 2–5 cm. During spraying, the sample was heated on a hotplate, maintained at a constant temperature of 100 °C. Once the coating was uniform, the film was dried on the hotplate at 100 °C for 1 h and then allowed to cool gradually to room temperature.

2.5 Photoelectrochemical performance test

The photoelectrochemical test was conducted using a 0.5 M Na_2SO_4 electrolyte solution and a three-electrode setup: SnO_2/S,N-CQDs as the working electrode (WE), Pt wire as the counter electrode (CE), and Ag/AgCl as the reference electrode (RE). Prior to testing, the electrolyte solution was purged with nitrogen gas for 30 min. A solar simulator was then used as the light source, with the light intensity calibrated to 100 mW/cm^2. Photocurrent density measurements were performed under both dark and light conditions using linear sweep voltammetry (LSV) with a PalmSens4 potentiostat, spanning a voltage range from −0.6 V to 1.6 V, with a minimum input current of 1 mA. Additionally, cyclic voltammetry (CV) was used to measure the photoconversion efficiency (PCE) and assess the active sites on the thin film surface.

2.6 Characterization

The samples were characterized using various techniques. X-ray diffraction (XRD) analysis was performed with a Bruker D8 Advance X'Pert3 Powder and Empyrean systems, using Cu Kα radiation (λ = 1.54 Å) over a diffraction angle (2θ) range of 20° to 90° to determine the crystal structure. Ultraviolet-visible spectroscopy (Jasco V-750) was used to measure the absorbance across different wavelengths. The morphology and microstructure of the samples were examined using field emission scanning electron microscopy (FE-SEM, Hitachi SU-3500) and high-resolution transmission electron microscopy (HR-TEM, 200 kV, Tecnai G2 20 S-Twin, FEI).

3 Result and discussion

3.1 Optical properties

The research investigates the optical properties of SnO_2/S,N-CQDs photoanodes using UV-Vis spectroscopy. As shown in Fig. 1, the absorbance of SnO_2 and SnO_2/S,N-CQDs photoanodes was measured with varying volumes of 2.5 mL, 5 mL, 7.5 mL, and 10 mL. The highest absorbance is observed in the UV-Vis region, where electron transfer occurs from the valence band (VB) to the conduction band (CB). Absorbance was measured directly in the 300–400 nm range, corresponding to the band gap (Fig. 2, Table 1). The UV-Vis spectrum shows an absorption peak at 400 nm, indicating that the SnO_2/S,N-CQDs photoanode effectively covers the UV-Vis region. This absorption behavior suggests that the photoanode exhibits high absorption quality.

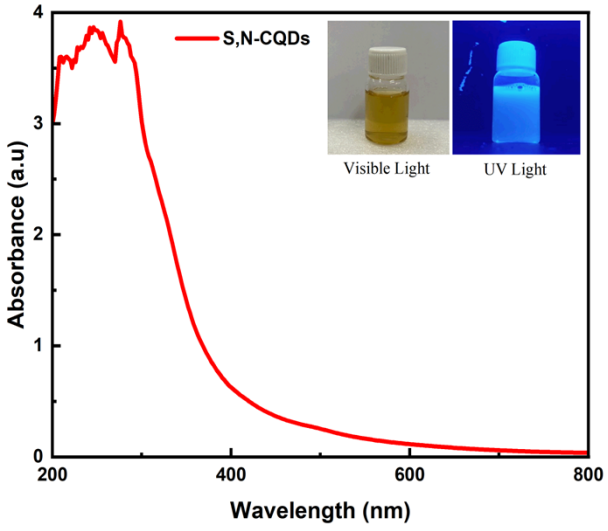

(a)

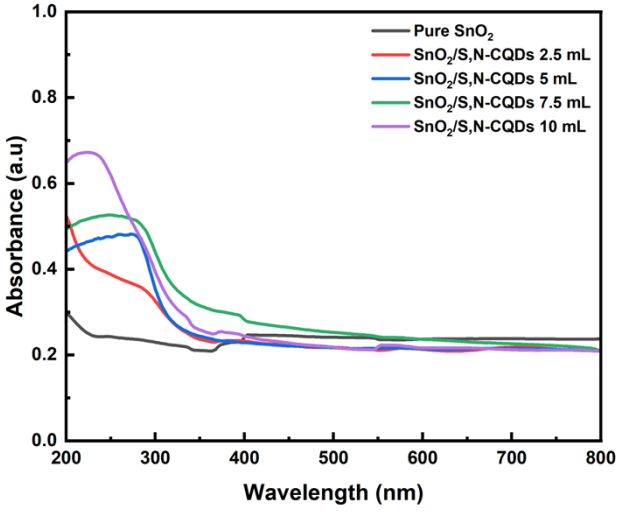

(b)

Fig. 1 UV-Vis absorbance spectra of (a) S,N-CQDs and (b) SnO_2/S,N-CQDs

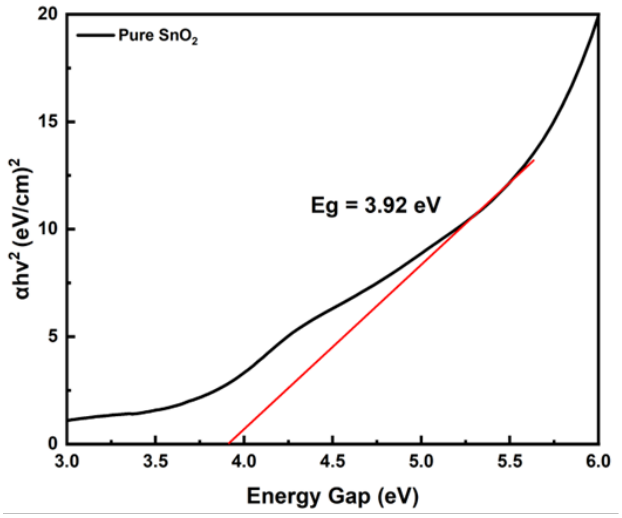

(a)

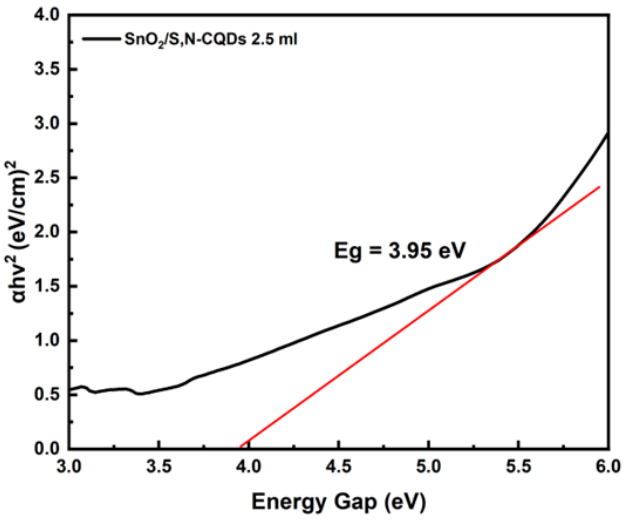

(b)

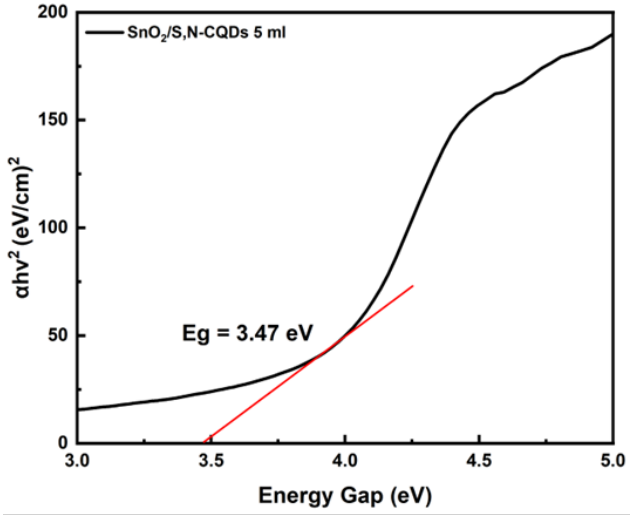

(c)

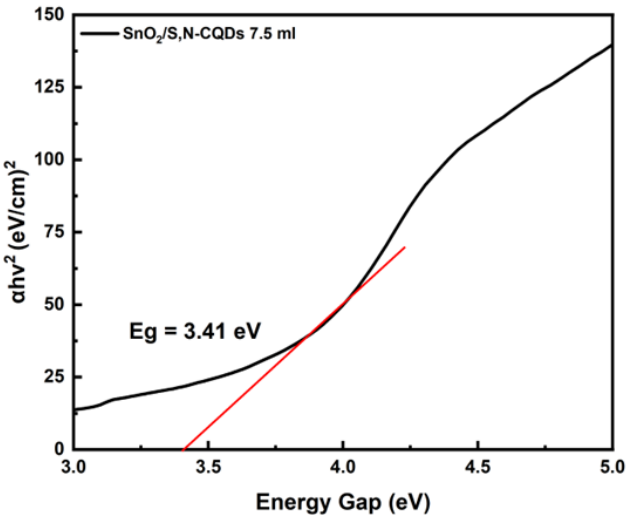

(d)

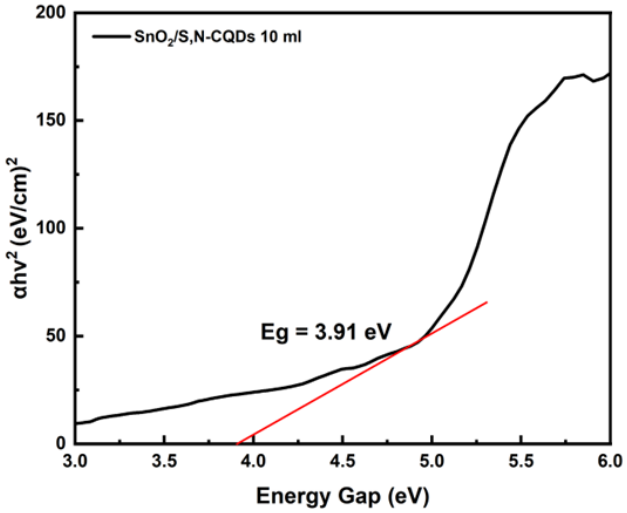

(e)

Fig. 2 Tauc plot of (a) pure SnO_2, (b) SnO_2/S,N-CQDs 2.5 mL, (c) SnO_2/S,N-CQDs 5 mL, (d) SnO_2/S,N-CQDs 7.5 mL and (e) SnO_2/S,N-CQDs 10 mL

Table 1 Band gap energy for all samples

Samples	Energy gap (eV)
Pure SnO_2	3.95
SnO_2/S,N-CQDs 2.5 mL	3.92
SnO_2/S,N-CQDs 5 mL	3.47
SnO_2/S,N-CQDs 7.5 mL	3.41
SnO_2/S,N-CQDs 10 mL	3.91

At 7.5 mL, the S,N-CQDs content is at an optimal level to enhance conductivity and support efficient charge transfer, enabling effective excitation and accumulation of electrons in the CB of SnO_2. This optimal interaction improves electron–hole separation and reduces recombination, resulting in higher photocurrent density. However, in the 10 mL sample, excessive S,N-CQDs lead to agglomeration on the SnO_2 surface, which not only blocks active light-absorbing sites but also creates recombination centers. This condition disrupts electron transport and prevents the effective accumulation of electrons in the CB, ultimately lowering the PEC performance [24].

At 10 mL excessive S,N-CQDs may lead to agglomeration on the SnO_2 surface, which can create recombination centers or hinder effective light absorption by blocking the active surface of SnO_2. An increase in the agglomeration of CQD nanoparticles resulted in a band shift. This indicates that agglomeration has a considerable impact on light absorption intensity and may also influence UV absorption and the photocatalytic performance of CQDs. Additionally, the observed wavelength shift due to agglomeration negatively affects the fluorescence properties [24].

3.2 XRD analysis

The XRD pattern of the SnO_2 layer sample is shown in Fig. 3. Based on the results of the XRD pattern owned by SnO_2 analyzed using HighScore Plus software [25], it is known to have the same diffraction peaks, namely at 26.5° (110), 32.4° (012), 34.1° (011), 37.7° (020), 51.5° (121), 54.5° (220), 61.5° (130), and 65.7° (031). The diffraction pattern was matched to a database [26] with reference code ICSD 98-016-9033 which is a reference code for SnO_2 with a rutile structure. Rutile unit cell with tetragonal symmetry was described with the space group $P4_2/mnm$ [27]. The highest diffraction peak is at peak (020) indicating that the pure SnO_2 samples and those already deposited by S,N-CQDs grow to the front of the FTO glass substrate. The appearances of small peaks around 27–28°, 38° and 49° can be correspond to existence of carbon deposited on surface of SnO_2 [28].

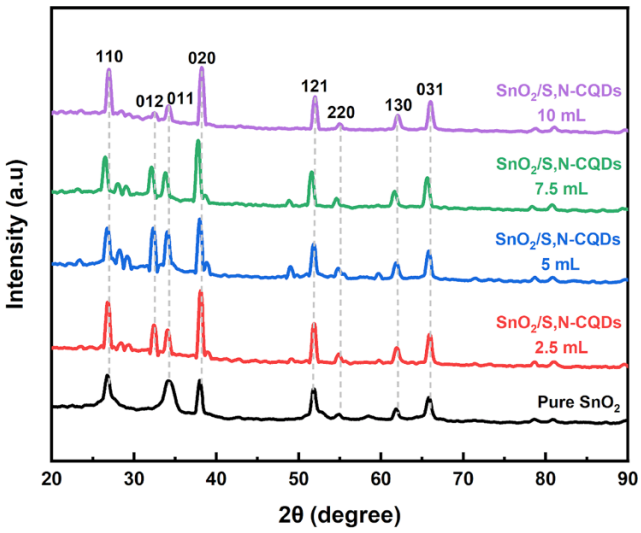

Fig. 3 XRD spectra of SnO_2 and SnO_2/S,N-CQDs

3.3 Morphological analysis

The morphology of SnO_2 grown on FTO substrates using the hydrothermal method was characterized by FE-SEM, as shown in Fig. 4 (a)–(c). The SnO_2 microstructure formed on the FTO substrate is spherical in shape, which is consistent with the morphology of SnO_2 modified with S,N-CQDs. However, the morphology of the thin film surface is less cracked than that of the FTO surface. The particle size distribution is relatively uniform, with an average diameter of 0.07 µm in the top view and 0.66 µm in the cross-sectional view, although some agglomeration is still present. Enhancing the QDs-PEC system primarily involves designing suitable structures to boost exciton generation to minimize charge recombination. In this study, S,N-CQDs are introduced as a modification material to improve the performance of the SnO_2 semiconductor [29].

The HR-TEM image of S,N-CQDs, shown in Fig. 4 (d), reveals that the synthesized nanomaterials are spherical and uniformly dispersed, with a size distribution ranging from 1 to 8 nm. The HR-TEM image of S,N-CQDs, shown in Fig. 4 (d), reveals that the synthesized nanomaterials are spherical and uniformly dispersed, with a size distribution ranging from 1 to 8 nm. The S,N-CQDs exhibit good dispersibility in water, without significant aggregation, suggesting that they are stabilized by functional groups [30, 31].

The composition of the S,N-CQDs solution consists of nitrogen content at 3.67 mL and a sulfur content of 1 mL based on elemental concentrations in algae from previous

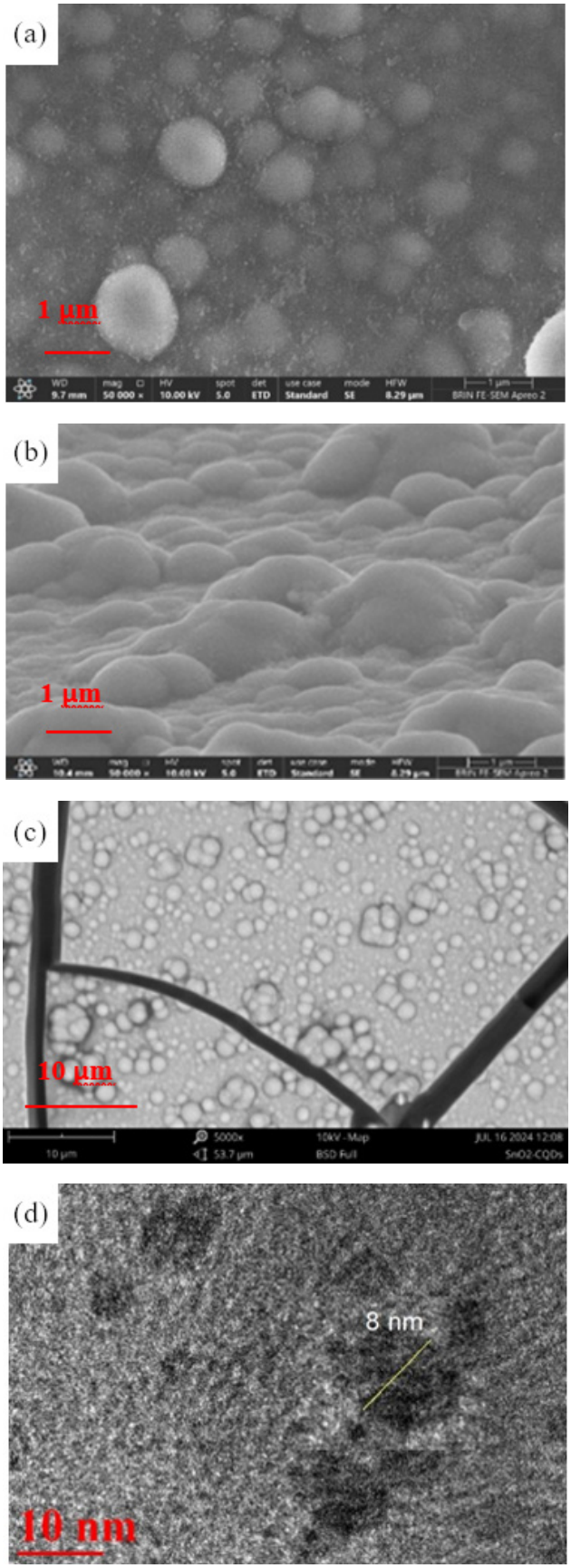

Fig. 4 (a) Top view FE-SEM image of SnO_2 thin film, (b) Cross-sectional view FE-SEM image of SnO_2 thin film, (c) SEM image of SnO_2/CQDs 7.5 mL, and (d) HR-TEM image of S,N-CQDs

studies [32, 33]. Based on the sulfur and nitrogen composition contained in the CQDs, the corresponding sulfur and nitrogen content in the modified SnO_2 photoanode was determined. For the SnO_2/S,N-CQDs with a 2.5 mL variation, the sulfur and nitrogen content was approximately 0.03 mL and 0.09 mL, respectively. In the 5 mL variation, the sulfur content reached 0.05 mL and nitrogen 0.18 mL. For the 7.5 mL variation, the sulfur content was 0.08 mL and nitrogen 0.27 mL. Finally, in the 10 mL variation, the sulfur and nitrogen contents increased to 0.1 mL and 0.37 mL, respectively [32, 33].

3.4 Surface analysis

The Raman spectrum (Fig. 5) of SnO_2/S,N-CQDs nanoparticles exhibits several bands at 580, 980, 1090, and 1570 cm^{-1}. The band observed at 630 cm^{-1} corresponds to the tetragonal symmetry of SnO_2 nanoparticles, while the band at 434 cm^{-1} is attributed to the bending mode of the Sn-O-Sn bond. Additionally, a band at 332 cm^{-1} is also observed in SnO_2. Vibrational modes at 372 cm^{-1}, associated with local lattice disorder, and at 560 cm^{-1}, indicative of oxygen vacancy (OV) concentration, are also present. The intensity of the peak at 560 cm^{-1} increases with a higher concentration of OVs. During air annealing, these oxygen vacancies are filled, leading to a decrease in peak intensity. In contrast, during vacuum annealing, oxygen atoms are removed from the film, resulting in an increase in peak intensity [34, 35].

3.5 Photoluminescence (PL) measurements

PL measurements were conducted to examine the charge recombination behavior and identify defects in the samples. Fig. 6 shows the PL results for a sample with an excitation wavelength of 325 nm. Generally, the addition of S,N-CQDs to the SnO_2 sample reduces the charge recombination density, as evidenced by the lower emission intensity compared to the pure SnO_2 sample. The peak observed in the PL spectrum corresponds to defects in SnO_2, such as OV or interstitial oxygen atoms (O_i). The reduction in this peak intensity in the S,N-CQDs-modified sample indicates a decrease in defect density [34, 36].

3.6 Photoelectrochemical performance

3.6.1 Linear sweep voltammetry

Photoelectrochemical testing using LSV, shown in Fig. 7, reveals different responses for SnO_2 photoanode samples and SnO_2/S,N-CQDs-modified photoanodes with varying volumes of S,N-CQDs addition. The potential measured relative to the Ag/AgCl reference electrode was converted

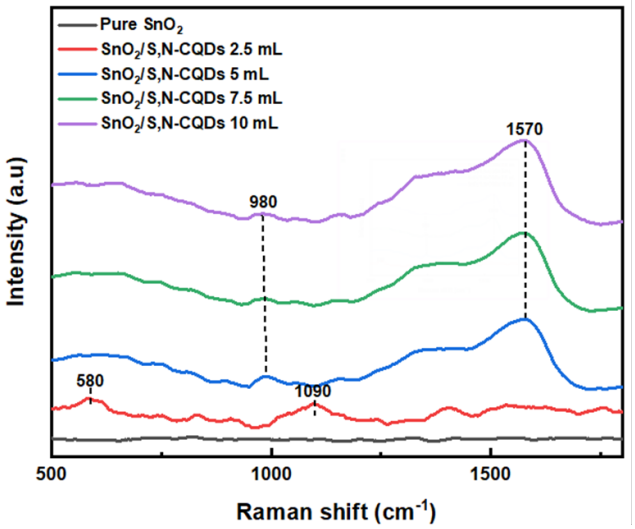

(a)

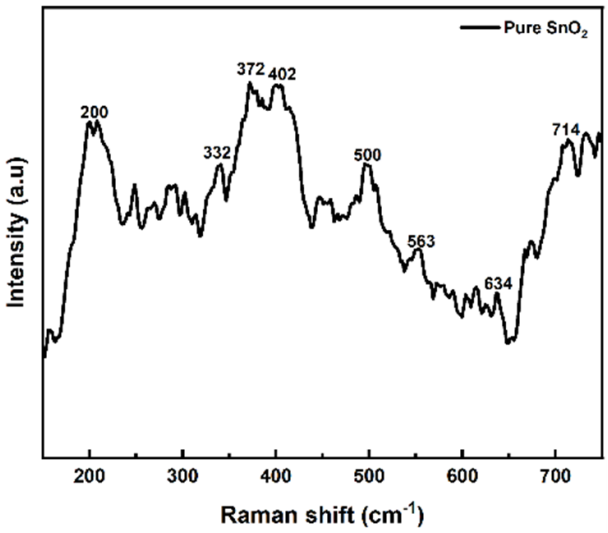

(b)

Fig. 5 Raman spectra of (a) SnO_2/S,N-CQDs and (b) SnO_2

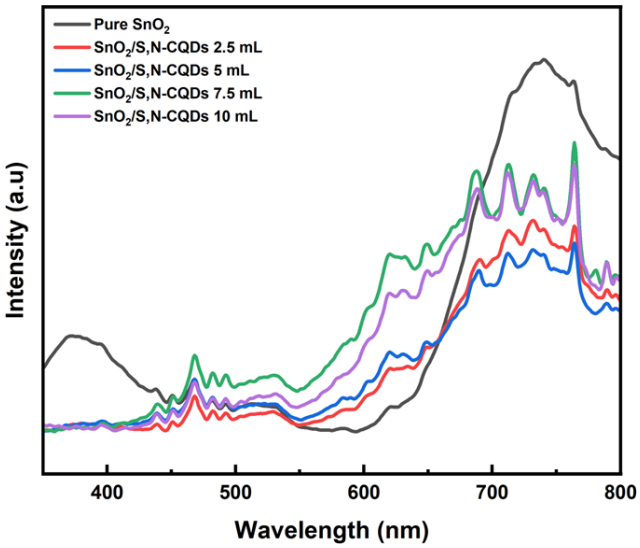

Fig. 6 PL spectra of pure SnO_2 and SnO_2/S,N-CQDs films

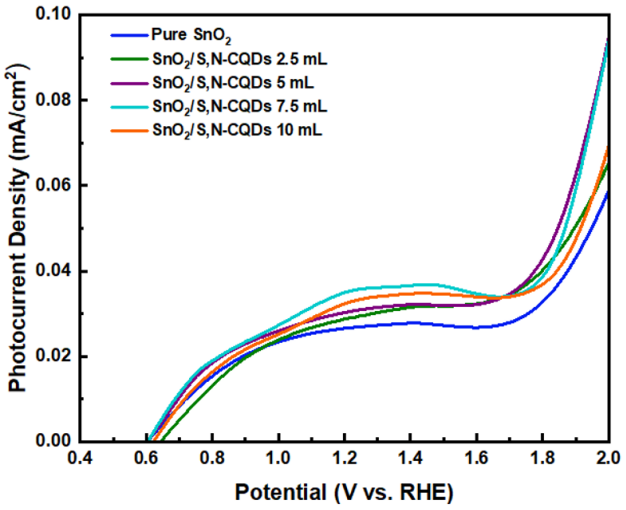

(a)

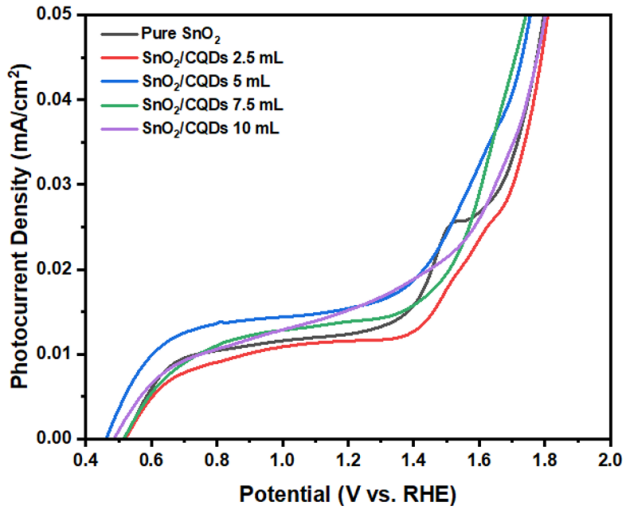

(b)

Fig. 7 LSV test results on (a) SnO_2/S,N-CQDs and (b) SnO_2/CQDs

to the reversible hydrogen electrode (RHE) scale using the Nernst equation:

$$E(\text{V vs. RHE}) = E(\text{V vs. Ag/AgCl}) + 0.21 + (0.059\ \text{pH}), \quad (1)$$

where E is the electrode potential.

The LSV testing results for the SnO_2/S,N-CQDs-modified photoanode with 7.5 mL of S,N-CQDs show the highest current density of 0.0356 mA/cm^2 at 1.23 V vs. RHE under a light intensity of 100 mW/cm^2. This is followed by SnO_2/S,N-CQDs with 10 mL of S,N-CQDs (0.0331 mA/cm^2), 5 mL of S,N-CQDs (0.0307 mA/cm^2), 2.5 mL of S,N-CQDs (0.0292 mA/cm^2), and pure SnO_2 (0.0268 mA/cm^2). These results indicate that the current density for SnO_2 photoanodes without S,N-CQDs modification increases upon the addition of S,N-CQDs.

N-doped CQDs and nitrogen/sulfur co-doped CQDs (N,S-CQDs) exhibit significantly higher fluorescence quantum efficiency and photocatalytic activity compared to pure CQDs [15, 16]. Additionally, the improved performance of N-doped CQDs has been positively correlated with the extent of nitrogen doping [17, 18]:

$$\text{ABPE} = \frac{J_{ph}\left(1.23\ \text{V} - V_b\right)}{P} \times 100\% , \tag{2}$$

where J_{ph} is the photocurrent density, V_b is the applied bias voltage, and P is the power density.

In the Applied Bias Photon-to-current Efficiency (ABPE) graph shown in Fig. 8, a higher ABPE value indicates better efficiency in converting light energy into electric current. The SnO_2 photoanode sample exhibits a maximum ABPE value of 0.0065% at 0.8 V vs. RHE, while the SnO_2/S,N-CQDs photoanode with the addition of 7.5 mL of S,N-CQDs shows a maximum ABPE value of 0.084% at 0.8 V vs. RHE. This demonstrates that the SnO_2/S,N-CQDs photoanode with 7.5 mL of S,N-CQDs exhibits superior performance compared to the pure SnO_2 photoanode and other S,N-CQDs variations in photoelectrochemical water splitting applications. These findings are consistent with several studies in the literature, which suggest that modifying SnO_2 photoanodes with S,N-CQDs enhances the light absorption capability of semiconductor materials with wide band gaps [37–39].

3.6.2 Chronoamperometry (CA) measurements

CA measurements were performed to assess the photostability of the samples, as shown in Fig. 9. This parameter provides insight into the stability of the material during the photoelectrochemical water splitting process. Photostability tests were conducted under both dark and light conditions, using an on/off method with a time interval of 60 s for a total duration of 420 s. As shown in Fig. 9, the SnO_2/S,N-CQDs sample with 7.5 mL of S,N-CQDs demonstrates the greatest stability compared to the other samples. This is evident from the consistent response observed under light and dark conditions, while other samples exhibit rapid charge recombination, indicated by fluctuating responses.

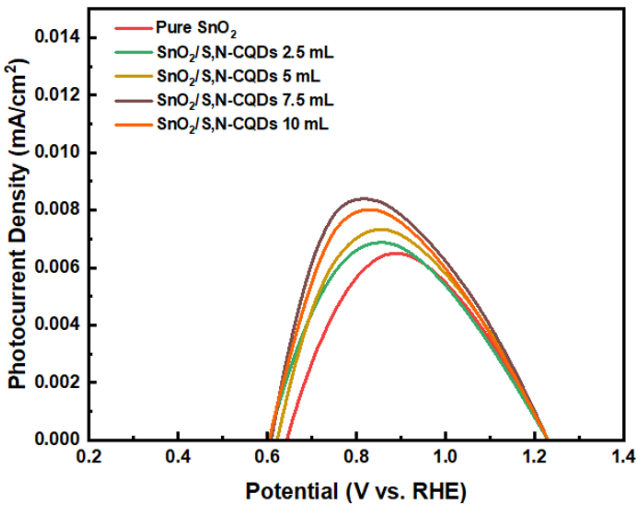

Fig. 8 ABPE test results on SnO_2/S,N-CQDs thin film photoanode samples

3.7 Cyclic voltammetry

CV testing is used to analyze the electrochemical response of the catalyst, its interaction with the electrolyte, and its catalytic activity [40]. The results of the CV tests on the samples are shown in Fig. 10, with scan rates of 15 mV, 30 mV, 45 mV, and 60 mV. The sample with 7.5 mL of S,N-CQDs shows the largest CV curve area, indicating better electrochemical performance. In contrast, the sample with 2.5 mL of S,N-CQDs shows the smallest CV curve area compared to the other samples. Higher scan rates in the CV tests can improve the accuracy of the sample's performance evaluation. A rectangular CV curve suggests good electric double-layer capacitance (C_{dl}), indicating efficient charge storage and stability [41, 42].

In the CV testing, the electrochemical surface area (ECSA) was analyzed. The ECSA of each system was evaluated based on the electrochemical C_{dl} of the catalyst surface. This capacitance was determined by analyzing the non-Faradaic capacitive current, which arises from double-layer charging, as a function of scan rate in CV measurements [43].

$$\text{ECSA} = \frac{C_{dl}}{C_s} \tag{3}$$

The ECSA value is determined by calculating the C_{dl} at various scan rates (v) [22, 44]. The ECSA data is processed using the linear regression method (Fig. 11), based on the C_{dl} values for each scan rate (v). Since the value of specific capacitance (C_s) is unknown, the relative change in ECSA is observed through the C_{dl} values. A higher C_{dl} value corresponds to a larger active surface area in the sample [45]. The sample with 7.5 ml S,N-CQDs variation has the most abundant active sites compared to the other samples.

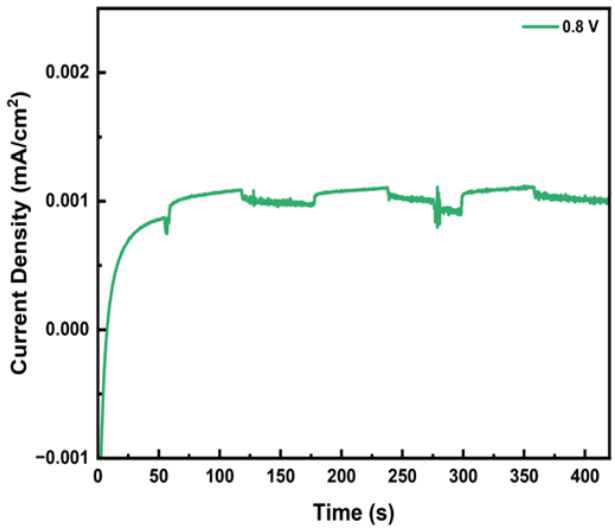

(a)

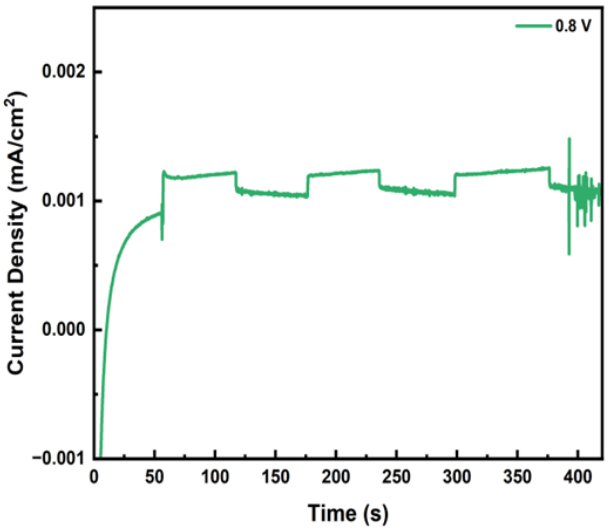

(b)

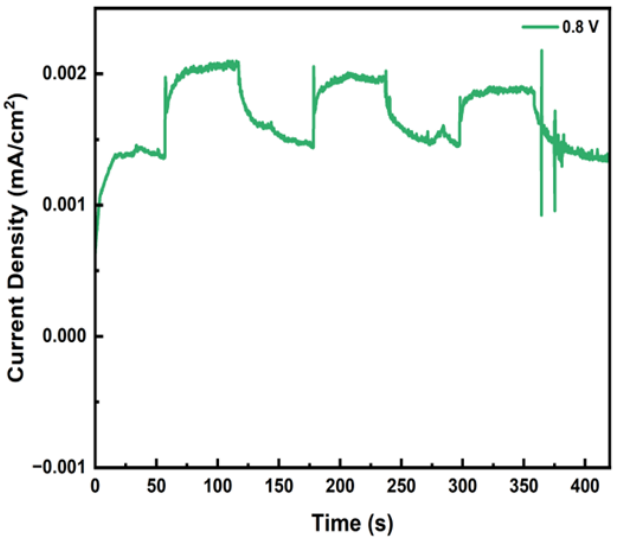

(c)

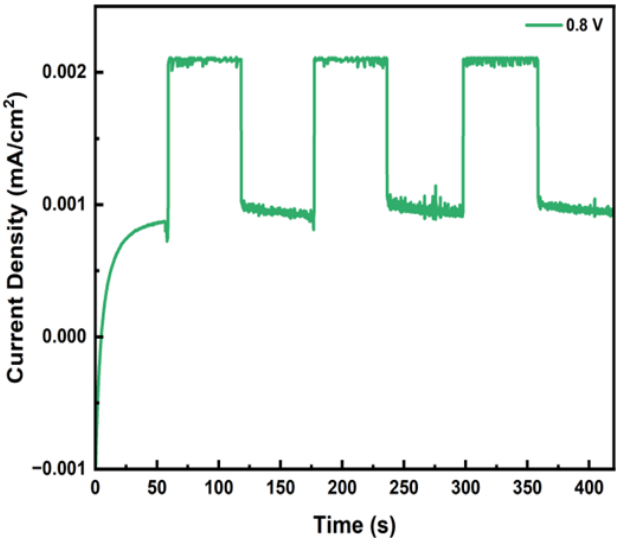

(d)

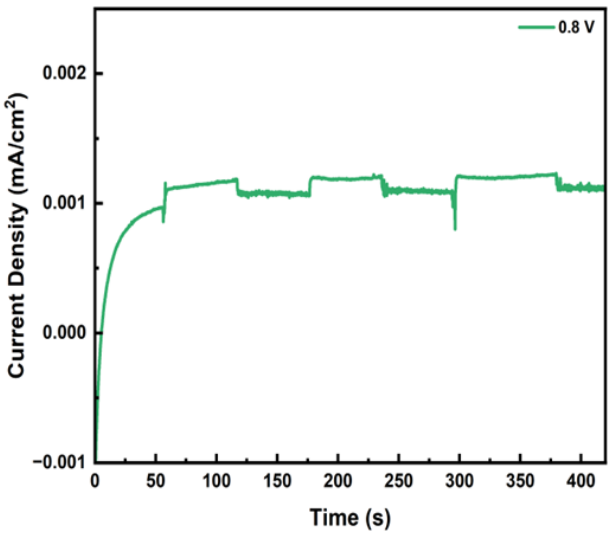

(e)

Fig. 9 Stability of (a) pure SnO_2, (b) SnO_2/S,N-CQDs 2.5 mL, (c) SnO_2/S,N-CQDs 5 ml, (d) SnO_2/S,N-CQDs 7.5 mL and (e) SnO_2/S,N-CQDs 10 mL

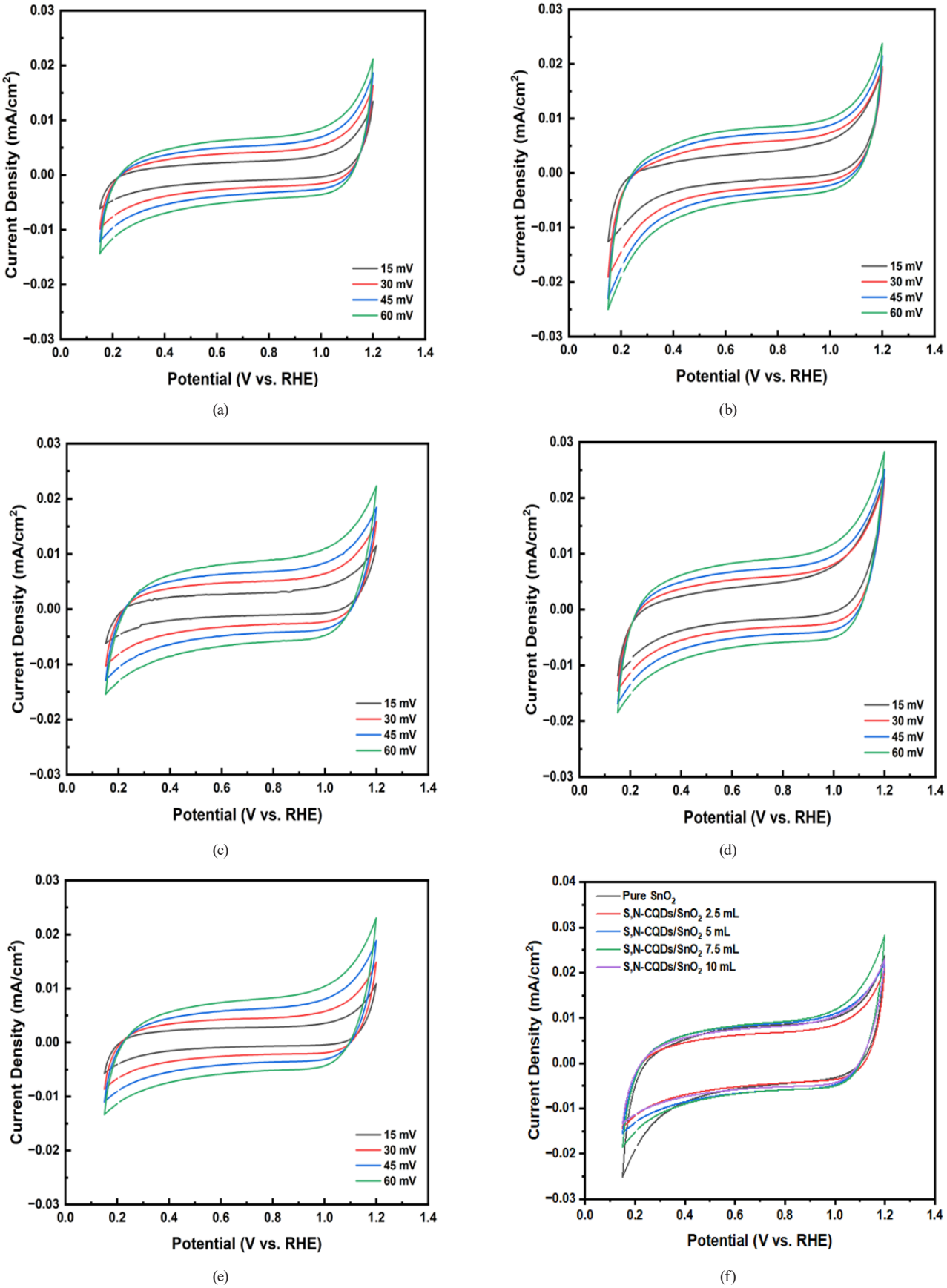

Fig. 10 CV test on samples of (a) pure SnO_2, (b) SnO_2/S,N-CQDs 2.5 mL, (c) SnO_2/S,N-CQDs 5 mL, (d) SnO_2/S,N-CQDs 7.5 mL, (e) SnO_2/S,N-CQDs 10 mL and (f) SnO_2/S,N-CQDs at 60 mV

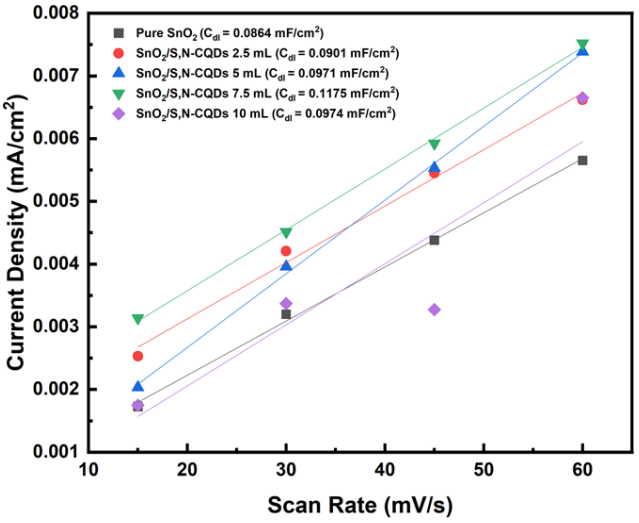

Fig. 11 Estimation of C_{dl} by plotting the current density variation against scan rate to fit a linear regression for SnO_2 and SnO_2/S,N-CQDs

4 Conclusion

Electron microscopy analysis reveals that SnO_2 particles on the FTO substrate exhibit a spherical microstructure, with a particle size distribution ranging from 0.04 to 0.1 µm. The average particle diameter is 0.073 µm in the top view and 0.066 µm in the cross-sectional view. HR-TEM characterization of the S,N-CQDs sample shows a uniform distribution of spherical particles, with sizes ranging from 1 to 8 nm. Modification of SnO_2 with S,N-CQDs at various concentrations resulted in an increased band gap, reduced charge recombination, and enhanced active sites on SnO_2, thereby improving the photoelectrochemical water splitting process. This material modification also boosts performance in photoelectron photocatalysis applications. In the SnO_2/S,N-CQDs photoanode modified with 7.5 mL of S,N-CQDs, LSV measurements showed a photocurrent density of 0.0356 mA/cm^2. Additionally, CV testing and ECSA measurements yielded a C_{dl} of 0.1175 mF/cm^2.

Acknowledgement

We would like to express our gratitude to the Universitas Pertamina – Universiti Teknologi PETRONAS Joint Research Program for their support, through research grant number 123/UP-R/SK/HK.01/VI/2023.

References

[1] Germscheidt, R. L., Moreira, D. E. B., Yoshimura, R. G., Gasbarro, N. P., Datti, E., dos Santos, P. L., Bonacin, J. A. "Hydrogen Environmental Benefits Depend on the Way of Production: An Overview of the Main Processes Production and Challenges by 2050", Advanced Energy and Sustainability Research, 2(10), 20170025, 2021. https://doi.org/10.1002/aesr.202170025

[2] Nazir, H., Louis, C., Jose, S., Prakash, J., Muthuswamy, N., Buan, M. E. M., …, Kannan, A. M. "Is the H_2 economy realizable in the foreseeable future? Part I: H_2 production methods", International Journal of Hydrogen Energy, 45(27), pp. 13777–13788, 2020. https://doi.org/10.1016/j.ijhydene.2020.03.092

[3] Wu, Z. L., Zhang, P., Gao, M. X., Liu, C. F., Wang, W., Leng, F., Huang, C. Z. "One-pot hydrothermal synthesis of highly luminescent nitrogen-doped amphoteric carbon dots for bioimaging from *Bombyx mori* silk – natural proteins", Journal of Materials Chemistry B, 1(22), pp. 2868–2873, 2013. https://doi.org/10.1039/c3tb20418a

[4] Bruhwiler, L., Basu, S., Butler, J. H., Chatterjee, A., Dlugokencky, E., Kenney, M. A., McComiskey, A., Montzka, S. A., Stanitski, D. "Observations of greenhouse gases as climate indicators", Climatic Change, 165(1), 12, 2021. https://doi.org/10.1007/s10584-021-03001-7

[5] Yoro, K. O., Daramola, M. O. "Chapter 1 - CO_2 emission sources, greenhouse gases, and the global warming effect", In: Rahimpour, M. R., Farsi, M., Makarem, M. A. (eds.) Advances in Carbon Capture: Methodes, Technologies and Applications, Woodhead Publishing. 2020, pp. 3–28. ISBN 978-0-12-819657-1 https://doi.org/10.1016/B978-0-12-819657-1.00001-3

[6] Mikhaylov, A., Moiseev, N., Aleshin, K., Burkhardt, T. "Global climate change and greenhouse effect", Entrepreneurship and Sustainability Issues, 7(4), pp. 2897–2913, 2020. https://doi.org/10.9770/jesi.2020.7.4(21)

[7] El ouardi, M., El Idrissi, A. Arab, M., Zbair, M., Haspel, H., Saadi, M., Ait Ahsaine, H. "Review of photoelectrochemical water splitting: From quantitative approaches to effect of sacrificial agents, oxygen vacancies, thermal and magnetic field on (photo)electrolysis", International Journal of Hydrogen Energy, 51, pp. 1044–1067, 2024. https://doi.org/10.1016/j.ijhydene.2023.09.111

[8] Yukesh Kannah, R., Kavitha, S., Preethi, Parthiba Karthikeyan, O., Kumar, G., Dai-Viet, N. V., Rajesh Banu, J. "Techno-economic assessment of various hydrogen production methods – A review", Bioresource Technology, 319, 124175, 2021. https://doi.org/10.1016/j.biortech.2020.124175

[9] Miao, S., Liang, K., Zhu, J., Yang, B., Zhao, D., Kong, B. "Hetero-atom-doped carbon dots: Doping strategies, properties and applications", Nano Today, 33, 100879, 2020. https://doi.org/10.1016/j.nantod.2020.100879

[10] Baker, S. N., Baker, G. A. "Luminescent Carbon Nanodots: Emergent Nanolights", Angewandte Chemie International Edition, 49(38), pp. 6726–6744, 2010. https://doi.org/10.1002/anie.200906623

[11] Iravani, S., Varma, R. S. "Green synthesis, biomedical and biotechnological applications of carbon and graphene quantum dots. A review", Environmental Chemistry Letters, 18(3), pp. 703–727, 2020. https://doi.org/10.1007/s10311-020-00984-0

[12] Li, H., Kang, Z., Liu, Y., Lee, S.-T. "Carbon nanodots: synthesis, properties and applications", Journal of Materials Chemistry, 22(46), pp. 24230–24253, 2012. https://doi.org/10.1039/c2jm34690g

[13] Bhunia, S. K., Pradhan, N., Jana, N. R. "Vitamin B1 Derived Blue and Green Fluorescent Carbon Nanoparticles for Cell-Imaging Application", ACS Applied Materials & Interfaces, 6(10), pp. 7672–7679, 2014. https://doi.org/10.1021/am500964d

[14] Liu, T., Cui, Z., Zhou, J., Wang, Y., Zou, Z. "Synthesis of Pyridinic-Rich N, S Co-doped Carbon Quantum Dots as Effective Enzyme Mimics", Nanoscale Research Letters, 12(1), 375, 2017. https://doi.org/10.1186/s11671-017-2149-y

[15] Ding, H., Wei, J., Xiong, H.-M. "Nitrogen and sulfur co-doped carbon dots with strong blue luminescence", Nanoscale, 6(22), pp. 13817–13823, 2014. https://doi.org/10.1039/C4NR04267K

[16] Ma, Z., Ming, H., Huang, H., Liu, Y., Kang, Z. "One-step ultrasonic synthesis of fluorescent N-doped carbon dots from glucose and their visible-light sensitive photocatalytic ability", New Journal of Chemistry, 36(4), pp. 861–864, 2012. https://doi.org/10.1039/c2nj20942j

[17] Briscoe, J., Marinovic, A., Sevilla, M., Dunn, S., Titirici, M. "Biomass-Derived Carbon Quantum Dot Sensitizers for Solid-State Nanostructured Solar Cells", Angewandte Chemie International Edition, 54(15), pp. 4463–4468, 2015. https://doi.org/10.1002/anie.201409290

[18] Yang, Z., Xu, M., Liu, Y., He, F., Gao, F., Su, Y., Wei, H., Zhang, Y. "Nitrogen-doped, carbon-rich, highly photoluminescent carbon dots from ammonium citrate", Nanoscale, 6(3), pp. 1890–1895, 2014. https://doi.org/10.1039/C3NR05380F

[19] Mallikarjuna, K., Rafiqul Bari, G. A. K. M., Vattikuti, S. V. P., Kim, H. "Synthesis of carbon-doped SnO_2 nanostructures for visible-light-driven photocatalytic hydrogen production from water splitting", International Journal of Hydrogen Energy, 45(57), pp. 32789–32796, 2020. https://doi.org/10.1016/j.ijhydene.2020.02.176

[20] Kumari, K., Ahmaruzzaman, M. "SnO_2 quantum dots (QDs): Synthesis and potential applications in energy storage and environmental remediation", Materials Research Bulletin, 168, 112446, 2023. https://doi.org/10.1016/j.materresbull.2023.112446

[21] Das, S., Jayaraman, V. "SnO_2: A Comprehensive Review on Structures and Gas Sensors", Progress in Materials Science, 66, pp. 112–255, 2014. https://doi.org/10.1016/j.pmatsci.2014.06.003

[22] Das, R., Bandyopadhyay, R., Pramanik, P. "Carbon quantum dots from natural resource: A review", Materials Today Chemistry, 8, pp. 96–109, 2018. https://doi.org/10.1016/j.mtchem.2018.03.003

[23] Gurau, S., Imran, M., Ray, R. L. "Algae: A cutting-edge solution for enhancing soil health and accelerating carbon sequestration – A review", Environmental Technology & Innovation, 37, 103980, 2025. https://doi.org/10.1016/j.eti.2024.103980

[24] Saafie, N., Sambudi, N. S., Wirzal, M. D. H., Sufian, S. "Effect of Hydrothermal Conditions on Kenaf-Based Carbon Quantum Dots Properties and Photocatalytic Degradation", Separations, 10(2), 137, 2023. https://doi.org/10.3390/separations10020137

[25] Malvern Panalytical "HighScore Plus software, (Version 5.3a)", Available at: https://www.malvernpanalytical.com/en/products/category/software/x-ray-diffraction-software/highscore-with-plus-option [Accessed: 11 July 2024]

[26] FIZ Karlsruhe GmbH "ICSD - the world's largest database for completely identified inorganic crystal structures", [online] Available at: https://icsd.products.fiz-karlsruhe.de/ [Accessed: 12 July 2024]

[27] Gupta, A., Kumar, A., Hegde, M. S., Waghmare, U. V. "Structure of $Ce_{1-x}Sn_xO_2$ and its relation to oxygen storage property from first-principles analysis", The Journal of Chemical Physics, 132(19), 194702, 2010. https://doi.org/10.1063/1.3425662

[28] Zhu, S., Liu, J., Sun, J. "Growth of ultrathin SnO_2 on carbon nanotubes by atomic layer deposition and their application in lithium ion battery anodes", Applied Surface Science, 484, pp. 600–609, 2019. https://doi.org/10.1016/j.apsusc.2019.04.163

[29] Jin, L., Zhao, H., Wang, Z. M., Rosei, F. "Quantum Dots: Quantum Dots-Based Photoelectrochemical Hydrogen Evolution from Water Splitting (Adv. Energy Mater. 12/2021)", Advanced Energy Materials, 11(12), 2170047, 2021. https://doi.org/10.1002/aenm.202170047

[30] Xu, M., Ruan, X., Yan, J., Zhang, Z., Yun, J., Zhao, W., Li, T., Shi, Y. "Synthesis, growth mechanism, and photoluminescence property of hierarchical SnO_2 nanoflower-rod arrays: an experimental and first principles study", Journal of Materials Science, 51(21), pp. 9613–9624, 2016. https://doi.org/10.1007/s10853-016-0169-0

[31] Zheng, F., Wang, Z., Chen, J., Li, S. "Synthesis of carbon quantum dot-surface modified P25 nanocomposites for photocatalytic degradation of *p*-nitrophenol and acid violet 43", RSC Advances, 4(58), pp. 30605–30609, 2014. https://doi.org/10.1039/C4RA02707H

[32] Álvarez, X., Cancela, Á., Freitas, V., Valero, E., Sánchez, Á., Acuña-Alonso, C. "Hydrothermal Carbonization and Pellet Production from *Egeria densa* and *Lemna minor*", Plants, 9(4), 425, 2020. https://doi.org/10.3390/plants9040425

[33] Obeid, F., Chu Van, T., Brown, R., Rainey, T. "Nitrogen and sulphur in algal biocrude: A review of the HTL process, upgrading, engine performance and emissions", Energy Conversion and Management, 181, pp. 105–119, 2019. https://doi.org/10.1016/j.enconman.2018.11.054

[34] Kumar, V., Bhawna, Yadav, S. K., Gupta, A., Dwivedi, B., Kumar, A., Singh, P., Deori, K. "Facile Synthesis of Ce–Doped SnO_2 Nanoparticles: A Promising Photocatalyst for Hydrogen Evolution and Dyes Degradation", ChemistrySelect, 4(13), pp. 3722–3729, 2019. https://doi.org/10.1002/slct.201900032

[35] Adjimi, A., Zeggar, M. L., Attaf, N., Aida, M. S. "Fluorine-Doped Tin Oxide Thin Films Deposition by Sol-Gel Technique", Journal of Crystallization Process and Technology, 8(4), pp. 89–106, 2018. https://doi.org/10.4236/jcpt.2018.84006

[36] Suthakaran, S., Dhanapandian, S., Krishnakumar, N., Ponpandian, N. "Hydrothermal synthesis of SnO_2 nanoparticles and its photocatalytic degradation of methyl violet and electrochemical performance", Materials Research Express, 6(8), 0850i3, 2019. https://doi.org/10.1088/2053-1591/ab29c2

[37] Wang, Z., Li, X., Tan, C. K., Qian, C., Grimsdale, A. C., Tok, A. I. Y. "Highly porous SnO_2 nanosheet arrays sandwiched within TiO_2 and CdS quantum dots for efficient photoelectrochemical water splitting", Applied Surface Science, 470, pp. 800–806, 2019. https://doi.org/10.1016/j.apsusc.2018.11.182

[38] Zhang, Z., Jiang, X., Mei, J., Li, Y., Han, W., Xie, M., Wang, F., Xie, E. "Improved photoelectrocatalytic hydrogen generation through $BiVO_4$ quantum-dots loaded on nano-structured SnO_2 and modified with carbon quantum-dots", Chemical Engineering Journal, 331, pp. 48–53, 2018. https://doi.org/10.1016/j.cej.2017.08.102

[39] Zhang, Z., Gao, C., Wu, Z., Han, W., Wang, Y., Fu, W., Li, X., Xie, E. "Toward efficient photoelectrochemical water-splitting by using screw-like SnO_2 nanostructures as photoanode after being decorated with CdS quantum dots", Nano Energy, 19, pp. 318–327, 2016. https://doi.org/10.1016/j.nanoen.2015.11.011

[40] Li, S., Thomas, A. "Chapter 12 - Emerged carbon nanomaterials from metal-organic precursors for electrochemical catalysis in energy conversion", In: Ran, F., Chen, S. (eds.) Advanced Nanomaterials for Electrochemical-Based Energy Conversion and Storage: Micro and Nano Technologies, Elsevier, 2020, pp. 393–423. ISBN 978-0-12-814558-6 https://doi.org/10.1016/B978-0-12-814558-6.00012-5

[41] Szkoda, M., Skorupska, M., Łukaszewicz, J. P., Ilnicka, A. "Enhanced supercapacitor materials from pyrolyzed algae and graphene composites", Scientific Reports, 13(1), 21238, 2023. https://doi.org/10.1038/s41598-023-48166-6

[42] Weng, Z., Zhu, J., Lu, L., Ma, Y., Cai, J. "Regulation of the electric double-layer capacitance of MoS_2/ionic liquid by carbon modification", Journal of Applied Electrochemistry, 53(4), pp. 689–703, 2023. https://doi.org/10.1007/s10800-022-01802-x

[43] McCrory, C. C. L., Jung, S., Peters, J. C., Jaramillo, T. F. "Benchmarking Heterogeneous Electrocatalysts for the Oxygen Evolution Reaction", Journal of the American Chemical Society, 135(45), pp. 16977–16987, 2013. https://doi.org/10.1021/ja407115p

[44] Connor, P., Schuch, J., Kaiser, B., Jaegermann, W. "The Determination of Electrochemical Active Surface Area and Specific Capacity Revisited for the System MnO_x as an Oxygen Evolution Catalyst", Zeitschrift für Physikalische Chemie, 234(5), pp. 979–994, 2020. https://doi.org/10.1515/zpch-2019-1514

[45] Liu, X., Wang, C. "In Situ Wet Etching of MoS_2@dWO_3 Heterostructure as Ultra-Stable Highly Active Electrocatalyst for Hydrogen Evolution Reaction", Catalysts, 10(9), 977, 2020. https://doi.org/10.3390/catal10090977